Macromolecular Chemistry and Physics
www.mcp-journal.de

All-Atom Molecular Dynamics Simulations of Poly(2,6-dimethyl-1,4-phenylene) Oxide: Validation of OPLS-AA Force Field for Conformational Behaviour in Vacuum and in Carbon Tetrachloride

Enzo Venezia, Finizia Auriemma, Odda Ruiz de Ballestreros, Gaetano Guerra, Giuseppe Milano, and Andrea Correa**

OPLS force field has been successfully validated for poly(2,6-dimethyl-1,4-phenylene) oxide (PPO) in comparison with quantum chemical results and available experimental data. The formation of stable polymer solvent complexes, where solvent molecules are hosted in closed loops, has been detected in molecular dynamics (MD) simulations of OPLS all-atom (OPLS-AA) models of diluted solutions of PPO in CCl_4. Estimations of free energy of solvation indicate an entropic stabilization of the polymer solvent complexes. A very high similarity of these structures with the intra-helical channels observed in the structure of PPO co-crystals suggests their possible role in the nucleation process inducing the crystallization of PPO from organic solvents.

1. Introduction

Polymer-solvent co-crystals (CC) are typically obtained through crystallization processes induced by solvents. Early examples from natural macromolecules are aqueous molecular compounds of cellulose and amylose with water. These compounds were formed through hydrogen bonds between water and the polymer chains. For this reason, in the past, it was generally believed that specific interactions, such as hydrogen bonds, were required to form such CCs. Later on, it was shown that also organic solvents could lead to a molecular recognition between the helical conformations of the chains of synthetic polymers and solvent molecules. Guenet has proposed to classify polymer solvent CCs according to molecular interactions in the following way: enthalpic CC formed through strong interactions (hydrogen bonds or electrostatic interactions), and entropic CC for which the driving force is molecular recognition involving weaker dispersive van der Waals type of interactions. Combinations of both types of interactions are also possible like for some poly(ethylene oxide) (PEO) CCs. PEO co-crystalline forms were also among the first discovered for a synthetic polymer[1–3] together with isotactic polystyrene (iPS).[4,5] A number of other CCs have been discovered for syndiotactic polystyrene,[6,7] poly[vinylidene fluoride], poly[vinyl chloride], Polyaniline, syndiotactic poly[p-methyl styrene], and other polymers as reported in reference.[8] For a complete overview of this research field the reader can refer to the book of Guenet.[8]

It is important to note that, for the majority of CC forms, guest removal causes a drastic rearrangement of polymer chains packing resulting in crystalline forms with densities that are typically greater than those of the amorphous phase. Only for two polymers, syndiotactic polystyrene[9–14] (s-PS) and poly(2,6-dimethyl-1,4-phenylene) oxide (PPO) (the repeating unit of PPO is reported below in **Scheme 1**),[9,10,11,12] the guest removal produces stable nano-porous crystalline structures where the space left by solvent molecules gives rise to cavities or nano-channels. These peculiar crystalline forms have been named as nano-crystalline (NC). Due to their peculiar properties, NC phases of s-PS and PPO, in the last three decades, have been subject of intensive studies involving several Italian research groups.

As for s-PS, at least three classes of co-crystalline forms have been identified, corresponding to the δ-clathrates, intercalates (also named δ-intercalates), and ϵ-clathrates. The removal of solvent molecules from the δ- and ϵ-clathrates generates NC forms

E. Venezia, G. Guerra
Department of Chemistry and Biology "A. Zambelli"
University of Salerno
Via Giovanni Paolo II, Fisciano 132–84084, Italy
F. Auriemma, O. R. de Ballestreros
Department of Chemical Sciences
University of Naples Federico II
Via Cintia, Complesso Monte Sant'Angelo 21, Naples 80126, Italy
G. Milano, A. Correa
Department of Chemical Engineering of Materials and Industrial Production
University of Naples Federico II
Piazzale Tecchio, 80, Naples 80126, Italy
E-mail: giuseppe.milano@unina.it; andrea.correa@unina.it

The ORCID identification number(s) for the author(s) of this article can be found under https://doi.org/10.1002/macp.202300120

DOI: 10.1002/macp.202300120

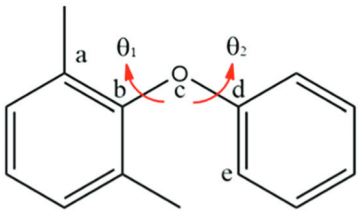

Scheme 1. Schematic representation of PPO dimeric model adopted in Density Functional Theory (DFT) and Molecular Mechanics (MM) gas phase calculations.

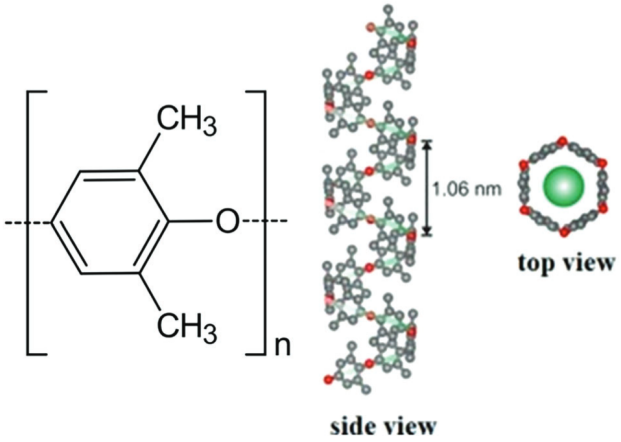

Figure 1. Schematic representation of PPO monomeric unit (left side) and a picture of side and top view of the intrahelical channel for a PPO chain (right side).

through small but significant rearrangement in the position of the chain axes, that are generally stable over a time long enough to make them suitable for numerous applications.[13–15] The molecular origin underlying the solvent-induced crystallization of the different CC and NC forms of sPS as a function of guest size, polarity, chemical structure and geometry has been also extensively investigated, as reviewed in refs. [13–15]. Due to their great propensity to include volatile organic compounds (VOCs) NC phases of s-PS have been considered for a variety of applications, including air and water purification, catalysis, and sensors.[16,17] Moreover, the inclusion of active antimicrobial, magnetic, photoreactive, or chiral-optical guests in polymeric films made of CC forms made these NC phases attractive for several advanced applications. Relevant aspects of s-PS have been rationalized using both Molecular Dynamics (MD) and Monte Carlo (MC) methods. In particular, the role of the host guest interactions on conformational selectivity and molecular orientations,[18–20] the anisotropic diffusion of penetrants,[21] and the gas sorption have been investigated by all-atom simulations.[21,22] Moreover, the complex polymorphic behavior of s-PS upon crystallization has been investigated by means of multiscale modeling approaches.[23]

Experimental studies about NC and corresponding CC forms of PPO (chemical structure of the repeating unit is reported on left side of **Figure 1**) are more recent. Indeed early studies of CC forms of PPO were reported in 2011[24] with further main activities only after 2016. It is important to note that both guest solubilities and diffusivities of NC PPO films are impressively higher than those obtained for NC s-PS films.

The ability of PPO to co-crystallize with guest molecules such as α-pinene, decalin, and tetralin has been well recognized for years.[25–29] These CC forms, presently addressed as class I co-crystals, feature chain in 4/1 helical conformation, interchain inclusion of guest molecules, for a maximum of 1 guest/4 monomeric units, and complete collapse of the crystalline scaffold (amorphization) upon guest removal. Only in recent years, a second class of PPO co-crystals, class II, able to form NC phases has been identified.[13–15,30,31] In particular, it has been shown that two well-distinguished CC forms of class II, named α and β forms, can be induced through suitable solvent treatments which, upon solvent removal, give rise to α and β NC forms. Class II CCs and NCs are characterized by similar structural features that include a high degree of disorder, as indicated by the presence of only a few and broad X-ray diffraction peaks and the presence of large amount of diffuse scattering. Compared with the CC and NC α forms, the CC and NC β forms show broader diffraction peaks and a slightly higher chain periodicity, equal to 0.53 nm for the α forms and 0.55 nm for the β form. The lack of long-range order, parallel and perpendicular to the chain axes, makes any attempt aimed at crystal structure determination of CC and NC α and β forms of PPO not straightforward, and even the determination of the chain conformation in the crystals may be deceptive. The hypothesis that the chain conformation in α and β forms of PPO corresponds to helices with large radius and average periodicity of 0.53 and 0.55 nm, respectively, has been suggested by the sign of dichroism for all vibrational peaks of α and β forms, which, for uniaxially stretched films, is opposite with respect to those of the amorphous phase.[32] In this hypothesis, the guest molecules in the CC α and β forms would be stacked inside the intrahelical channel, rather than in the inter helical space. A picture of this chain conformation is reported on the right side of Figure 1. The presence of helices with large diameter hosting in the inter-helical space guest molecules, indeed, complies well with the high diffusivity achieved by low molecular mass solvents across PPO films in α and β NC forms, when the chain axes are preferentially oriented perpendicularly to the film plane.

Most relevant results on crystallization of PPO from solvents, NC and related CC forms of PPO have been very recently reviewed by some of the authors of the present paper.[32]

Due to the recent advent of NC and related CC forms of PPO, simulation studies and molecular models of PPO have been much less explored. The aim of the present paper is to test the conformational behavior of an all-atom model of PPO based on OPLS-AA force field[33] in comparison with high level quantum chemical calculations. The same all-atom model has been used for a preliminary single chain study (very diluted solution) of PPO in carbon tetrachloride, a solvent known to induce crystallization of CC forms. Previous few atomistic MD studies have been addressed to provide structures for amorphous PPO. In particular, a first early study of permeability for an atomistic model of amorphous PPO for four different gas molecules (O_2, N_2, CH_4, and CO_2) has been reported by Fried et al. using COMPASS force field.[34] More recently, molecular structures of amorphous PPO have been proposed by Singh et al. using the GROMOS 45a3 force-field and validated against experimental solubility parameter.[35] Sweere et al. proposed a multi-scale protocol employing a mapping/reverse-mapping procedure able to generate all-atom structures of amorphous PPO.[36] Coarse grained

(CG) cationic models have been reported to study PPO based materials for anionic exchange in water solutions by MD and DPD simulations.[34,37,38]

With these precedents, the choice of OPLS-AA has been motivated by the ability of this force field to provide reliable models for the most common organic solvents and for synthetic polymers.[39] According to these features, such a model is expected to be a good candidate to describe the mechanism of molecular recognition between PPO helical conformations and solvent molecules leading to the crystallization of CC phases.

The paper is organized as follows: in the Results section, a systematic quantum mechanical conformational study is reported together with molecular mechanics results (first subsection). A first test application of the proposed force field for liquid diphenyl ether validated by comparison of density and heat of vaporization (second subsection) with available experimental results is also reported. The last part of Results section is devoted to the preliminary application of the proposed PPO model to simulations of diluted solution in CCl_4 (one of the solvents inducing co-crystallization and achievement of the NC phase by solvent extraction). Finally, in the Conclusion section, the main results are summarized and possible implications of the simulation results in the mechanism of CCl_4 induced co-crystallization of PPO are discussed. Both, computational details and simulation methods are briefly reported in the Methods section.

2. Experimental Section

2.1. Quantum Chemistry Calculations

Quantum chemistry calculations were performed using the Density Functional Theory (DFT) by Gaussian09 package.[40] The electronic configuration of all atoms was described by 6–31G(d,p) basis set.[41–47] The B3LYP[48] functional was employed for rigid potential energy scan and geometry optimizations. For the rigid potential energy surface scan (gaussian keyword = Scan) a step of 10 degree was employed for the two dihedral angles considered, see Scheme 1, (going from 0 to 360 degrees).

2.2. MM Calculations

Molecular Mechanics (MM) calculations were performed using GROMACS package.[49] OPLS-AA force field parameters[33,50] were used to describe the system. Non bonded and bonded parameters are reported in Supporting Information section. The conjugate gradient algorithm (cg), as implemented in GROMACS, was used for energy minimizations. The minimization procedure was considered converged when the maximum force was calculated to be smaller than 10.0 kJ mol^{-1} nm^{-1}. For rigid scan a step of 10 degrees was employed for both torsional angles, going from 0 to 360 degrees.

2.3. MD Simulation Parameters

To model the DPE condensed phase, PPO chains, and CCl_4, we adopted the OPLS-AA force-field.[33,50] In the Supporting Information, SI, the full list of used parameters for bonded and non-bonded interactions is reported. In Scheme S1 (Supporting Information), the chemical skeleton of the PPO repeating unit is reported together with atom type tags. For all simulated systems, the chains are composed of 18 repeating units. Phenyl groups are used as chain's terminals. All atomistic simulation have been performed in the NPT ensemble by using GROMACS package.[49] A time step of 2 fs was used for all simulations. The non-bonded interactions modeled by Lennard-Jones potentials were truncated after a cut-off of 1.1 nm and the same distance was used as the switching distance for the particle mesh Ewald (PME) algorithm for computing Coulomb interactions.[51,52] Although the OPLS-AA force field was not developed for use with PME, extensive studies on water models and proteins in water have shown that correspondence of simulation results with experimental data improves considerably when long-range interactions are taken into account explicitly, irrespective of the force field used.[53,54] Analytic corrections to pressure and potential energies were made to compensate for the truncation of the Lennard-Jones interactions. In the production simulations, we used the Nosee-Hoover algorithm for temperature coupling.[55,56] For production simulations at constant pressure, the Parrinello-Rahman pressure coupling[57] algorithm was used with compressibility set to 5×10^{-5} bar^{-1} and a time constant of 5 ps. All bonds were constrained using the LINCS algorithm[58,59] for all molecules. Two independent replicas of a systems containing 1 PPO chain and 5801 CCl_4 molecules in periodic boundary conditions have been considered, at 300 Kelvin, see **Table 1** for details. The two replicas were first equilibrated for a simulation time of 10 ns, then production runs of 120 ns were performed. For DPE simulations a box containing 471 molecules, in pbc, has been first equilibrated and then sampled for 32 ns at 303.15 Kelvin and 1 atm. A comparison between experimental and calculated bulk properties for DPE is reported in **Table 2**.

Table 1. Simulated systems.

System	No. of. Chains	No.of solvent molecules	Total no. particles	Box size (nm) [$x = y = z$]	Time [ns]	T [K]
DPE	0	471	10 833	4.95904	32	303.15
PPO/CCl_4[a)]	1	5801	29 329	9.83789	120	300.00

[a)] For PPO/CCl_4 two independent simulations have been conducted

Table 2. Comparison between experimental and calculated bulk properties for DPE.

System	ΔH_{vap} [kj mol^{-1}]	ρ [gdm^{-3}]	Υ [10^{-3} Nm^{-1}]	T [K]
DPE (experimental)	58.42	1066.1	38.24	303.15
DPE (calculated)	63.0	1081.0	32.6	303.15

3. Results

3.1. DFT and Molecular Mechanics Force Field Validation

We have validated OPLS-AA force field parameters, based on DFT calculations, for PPO dimer-like molecular model reported in Scheme 1. The PPO structures can be viewed as a large conjugated system with two points of rotation for each dimeric unit, namely the torsion angles θ_1 and θ_2.

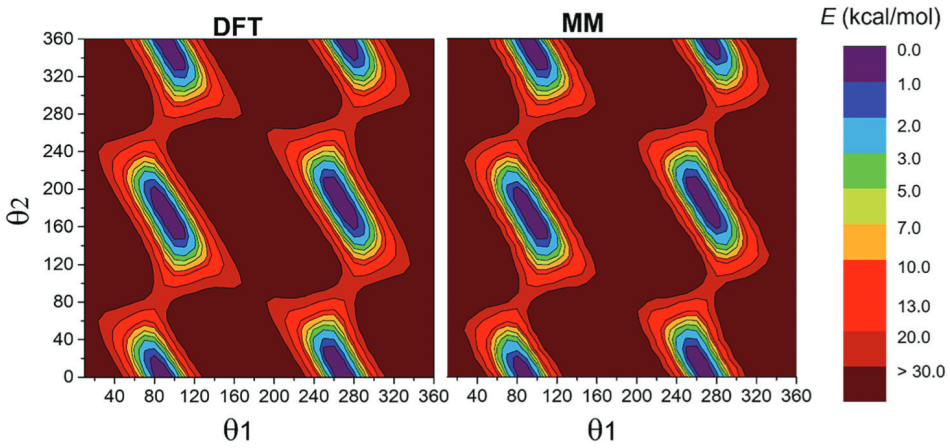

Figure 2. Rigid scan of the torsional energy surface of PPO dimeric model (see Scheme 1) calculated at the B3LYP/6-31G(d,p) level (left side) and MM/OPLS-AA force field (right side).

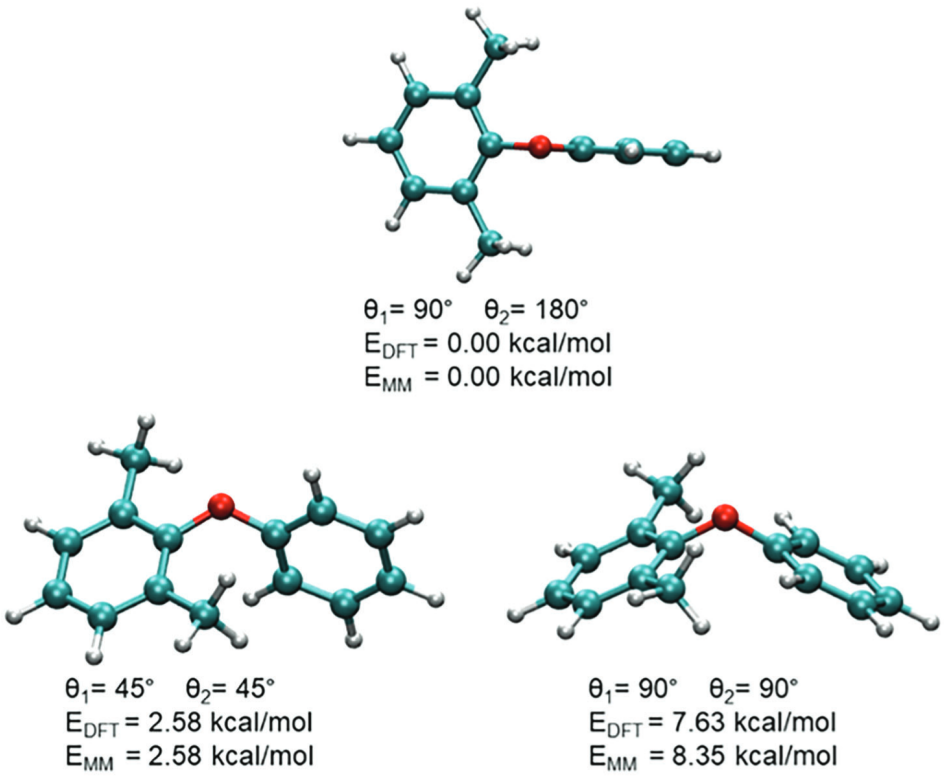

Figure 3. Selected, optimized structures of PPO dimeric model are depicted. The most stable conformer ($\theta_1 = 90°$ and $\theta_2 = 180°$) has been used as zero energy reference (top view).

In order to explore the conformational space around these two dihedral angles rigid conformational scans have been performed at B3LYP/6-31G(d,p) level of theory (Potential Energy Surface, PES calculations) and OPLS-AA force-field. To have a reasonable starting point for the rigid scan analysis, a guess structure, featuring $\theta_1 = 90$ and $\theta_2 = 180$ degrees, was fully optimized at the B3LYP/6-31G(d,p) level of theory, thus, frequencies were calculated in order to ensure its real minima nature and no imaginary frequencies were detected. This structure was used as starting point for both, B3LYP and OPLS-AA, PES calculations reported in **Figure 2**. The comparison between the two PESs clearly shows an excellent agreement in the different energy regions identification.

Moreover, from the DFT rigid scan calculation three different conformations were extracted and further optimized, at DFT and MM level, relaxing all degrees of freedom with the exception of θ_1 and θ_2, see **Figure 3**. According to the PES and as reported by Auriemma and co-workers,[32,60] the lowest energy structures correspond to θ_1 and θ_2 values of 90 and 180 degrees, and a slightly higher energy conformation (≈2.5 kcal mol^{-1}) was

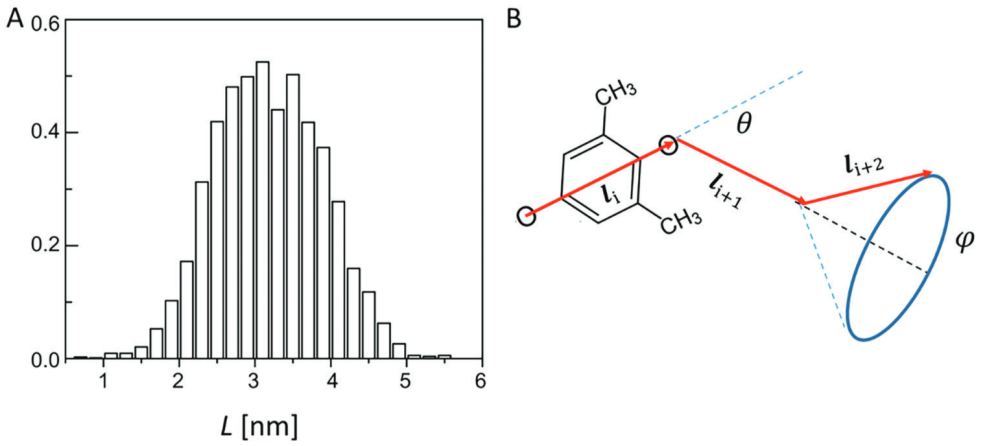

Figure 4. A) End-to-end distance distribution calculated from two independent MD simulations at 300 K. B) Schematization of freely rotating Gaussian chain for a PPO model. The segment length of 0.5528 nm can be calculated as two times the sum of C—O and aromatic C—C equilibrium distances of the OPLS-AA model. The angle $\theta = 69°$ is the supplementary of the equilibrium valence C—O—C angle 111°.

identified for θ_1 and θ_2 values of 45 degrees. A third, high energy, structure with θ_1 an θ_2 values of 90 degrees, was tested. MM and DFT relative energies, as well as DFT optimized structures are shown in Figure 3. Comparison between MM and DFT results clearly shows that OPLS-AA force field parameters reproduce very well the conformational behavior of PPO dimers not only for the low energy conformers, but also for the high energy conformation ($\theta_1 = \theta_2 = 90$ degrees) the OPLS-AA force field can reproduce the relative energy with an error lower than 1 kcal mol^{-1}, see Figure 3 for details. Beside the previously described in vacuum DFT calculations, as further validation of the employed forcefield including the adopted torsion parameters, condensed phase MD simulations of diphenyl-ether (DPE) have been performed at room temperature. Good agreement between experimental and calculated density, heat of evaporation, and surface tension has been obtained. More details about the adopted model are reported in the Methods and Supporting Information section.

3.2. MD Simulations in Condensed Phase

The distribution of the end-to-end distances (L) calculated from two independent MD simulation trajectories is reported as a histogram in **Figure 4**A. Values of L are symmetrically distributed around the average value of 3.2 ± 0.7 nm. As reported by Akers et al., chain dimensions of PPO have been estimated by Stockmayer-Fixman[61,62] and Kurata-Stockmayer[63] through extrapolation procedures in diluted solutions of different organic solvents including CCl_4. Their assumption about the segment length (l) (see Figure 4B) of 0.54 nm well compares with the one corresponding to equilibrium bond distances (two times the sum of C—O and aromatic C—C distances) of the here employed OPLS-AA force field of 0.5528 nm. Moreover, the same authors observed that experimental data obtained from CCl_4 solutions were compatible with the behavior of a Gaussian chain having completely free rotation about bonds. This means that all possible values of the dihedral angle φ as sketched in Figure 4B are equally probable. This feature lets Akers et al. conclude that PPO chains are tightly coiled in CCl_4. The average value of 3.2 nm

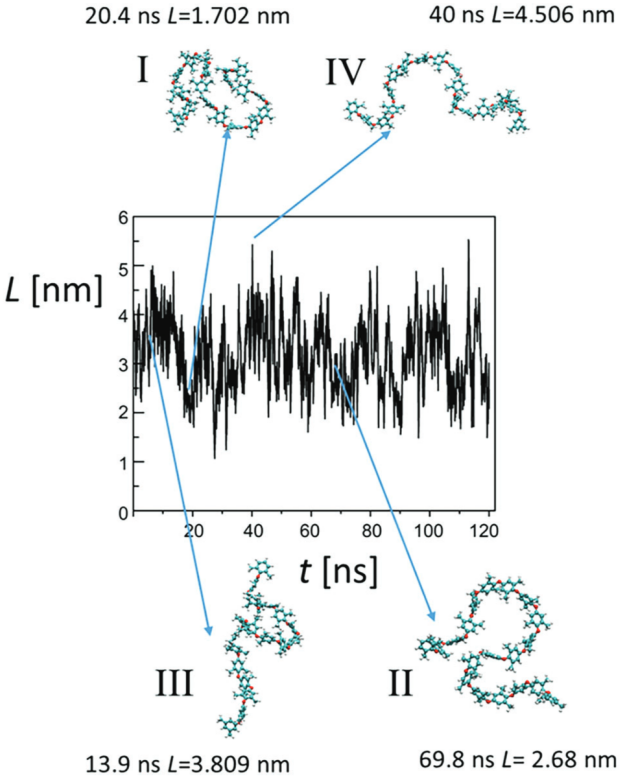

Figure 5. Time behavior of end-to-end distance L for one of the two independent MD simulations of a single PPO chain in CCl_4. Representative snapshots of chain conformations are also reported. CCl_4 molecules are not reported for clarity.

calculated from our MD simulations well compares with experiments and then with the analytical value obtained for freely rotating Gaussian chain equal to 3.32 nm, calculated considering the equilibrium bond distances and valence angle C-O-C values for the employed OPLS-AA force field.

The time behavior of the end-to-end distance (L) of the polymer chain for one of the two independent MD simulations,

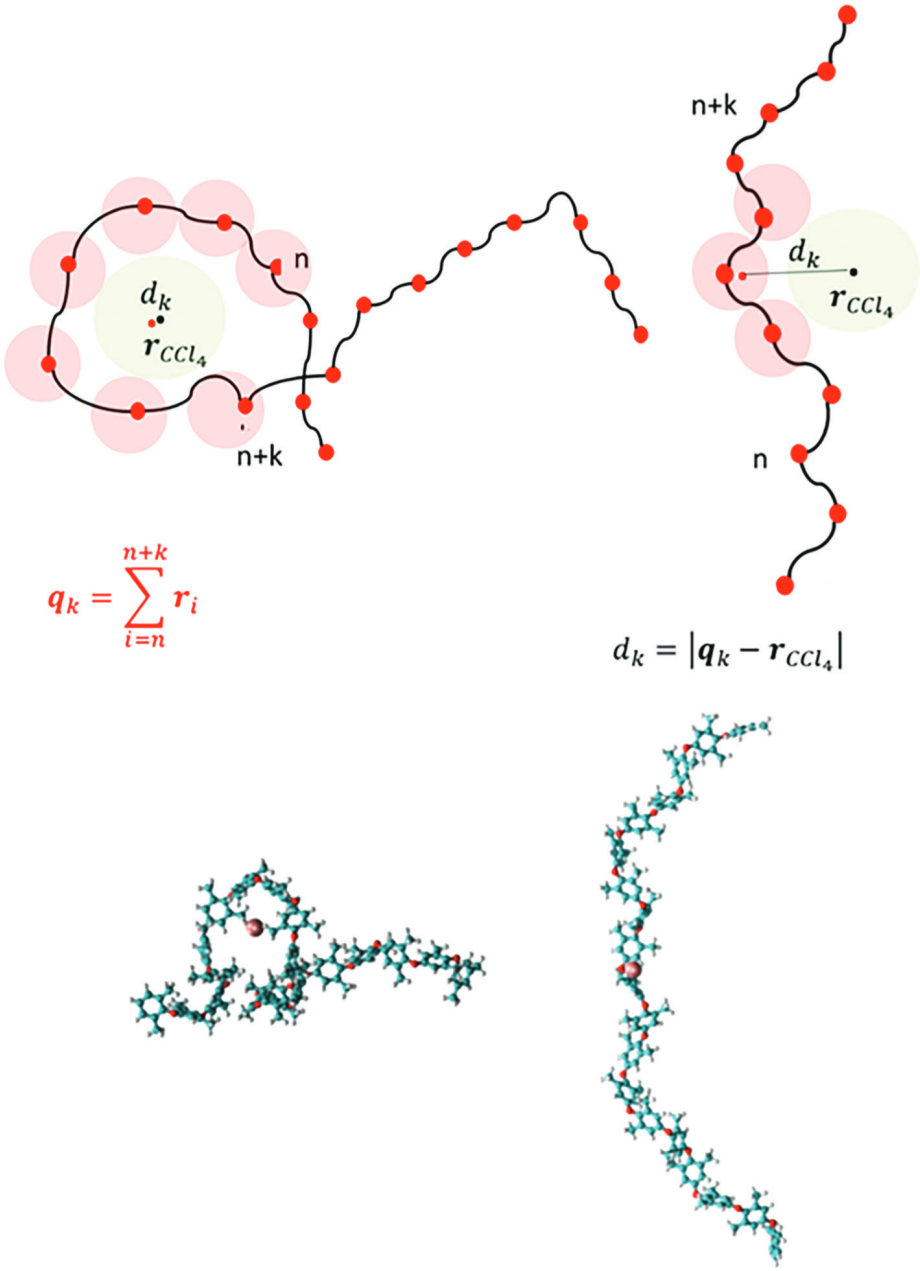

Figure 6. Top panel: schematizations of PPO chain (red dots represent oxygen atoms) in a loop (left side) and open (right side) conformation together with definition of the order parameter d_k as distance between the center of mass calculated for a group of k successive oxygen atoms and the center of mass of CCl_4 molecules. As schematized on the left side, for a loop conformation d_k will be small, while, for an open conformation, the same parameter will be large and close to the sum of atomic radius of an atom of the backbone and the molecular radius of CCl_4. Lower panel: position of the center of mass $\boldsymbol{q}_k$ (for $k = 7$) for a loop conformation (left side) and for an extended conformation (right side). The position of q_k is highlighted by a purple sphere.

together with some representative snapshots of the PPO chains, are reported in **Figure 5**. From Figure 5 it is possible to see that low values of L (below 3 nm) correspond to highly coiled conformations presenting two "closed loops" along the polymer chain (conformations I and II), while the presence of one "closed loop" gives values of $L \approx 3$ nm (conformation III).

Finally, conformations showing values of L larger than 4 nm correspond to open conformations (conformation IV). The picture obtained from MD simulations herein reported is in both quantitative and qualitative agreement with the microscopic behavior supposed by Akers et al. on the basis of experiments. More deep analysis of MD trajectories has been performed in order to have a more detailed molecular view of the observed puzzling behavior. In particular, from initial inspections of MD trajectories it is clear that the closed loops formed by the chains in coiled conformations have a size compatible with one or two CCl_4

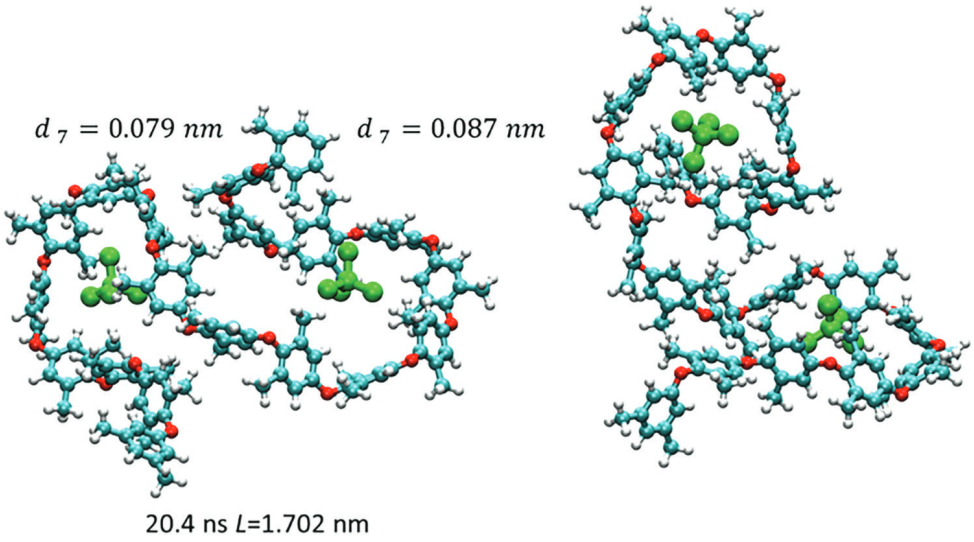

Figure 7. Conformation I of a PPO chain together with the two CCl4 molecules hosted in the two loops in two different projections. End-to-end distance L and values for d_7 for both solvent molecules are also reported. The conformation is observed after 20.4 ns along the MD trajectory.

molecules. In order to detect this type of molecular complexes from atomic trajectories a proper order parameter has been defined. As depicted in **Figure 6**, a good order parameter is the distance between the center of mass (COM) of a group of successive k repeating units of PPO and the COM of CCl_4.

This distance in the case of chain loops (where the COM is in the middle of the loop) will be very small/close to zero. On the contrary, in open conformations (where the COM is located closer to the backbone) this distance will be larger than the sum of the molecular radius of CCl_4 and the atomic radius of some of the atoms of the backbone. Our choice, according to the loop structures observed along two independent simulations (the number of oxygen atoms involved in one loop goes from 5 to 10), was $k = 7$ and with parameter $\boldsymbol{q}_7$ calculated using the positions of groups of seven successive oxygen atoms along the PPO chain. As a cut off distance for d_7 to detect a molecule of CCl_4 included into a loop a good choice is $d_{\text{cutoff}} = 0.1$ nm. In the lower panel of Figure 6 the position of $\boldsymbol{q}_7$ as a purple sphere for a typical loop configuration (left side) of the PPO chain located around the center of the loop and far from the chain backbone is reported. The position of the same vector for an extended conformation where $\boldsymbol{q}_7$ is close to backbone atoms is reported on the right side of the same figure. This type of analysis allows establishing that coiled conformations of PPO can host a solvent molecule inside their loops. The formation of such molecular complexes between PPO chains and solvent molecules has been visualized along both calculated trajectories for all coiled conformations.

For example, conformations at low L such as conformation I of Figure 5 (L = 1.702 nm) hosts a CCl_4 in each loop. In **Figure 7** the PPO in this conformation together with the two solvent molecules included in the two loops are reported (values of d_7 for both solvent molecules are also reported in the same figure). It is interesting to note that in conformation I each loop lies on one plane and the two planes containing the loops are almost orthogonal. The two loops have different sizes in terms of number of oxygen atoms involved in the loop, which is five or six for the first loop reported on the left side of Figure 7 and about eight for the second loop reported on the right side of Figure 7. Favorable non-bonded interactions (from both Lennard-Jones and Coulomb potentials) between chlorine atoms of both CCl_4 molecules and methyl groups of PPO chains have been detected. In particular, short distances between chlorine and hydrogen atoms of methyl groups (ranging from 0.27 to 0.13 nm) can be calculated for conformation I.

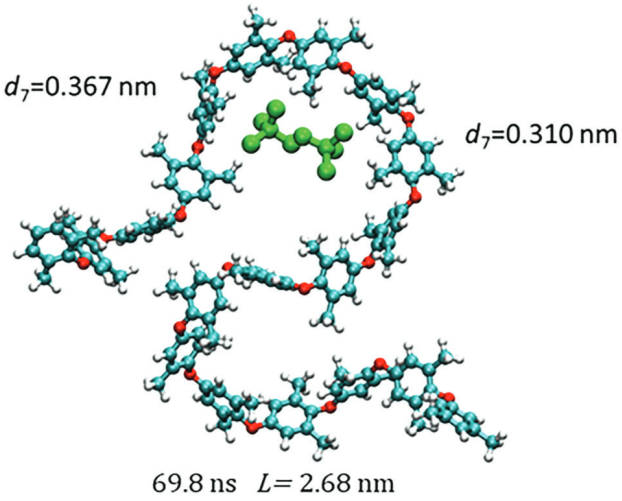

Figure 8. Conformation II of PPO chain together with the two CCl_4 molecules hosted in one loop. End-to-end distance L and value for d_7 for both solvent molecules are also reported. The conformation is observed after 69.8 ns along the MD trajectory.

Visual inspections of MD trajectories, filtering the guest molecules using the cut-off distance on d_7, show that host/guest structures are highly fluxional. The loop, together with the guest molecule, can slide along the chain, can fuse into a larger loop hosting two molecules, or can disappear in an open structure like conformation IV reported in Figure 5 or can fold into an empty loop expelling the solvent molecule. The conformation II,

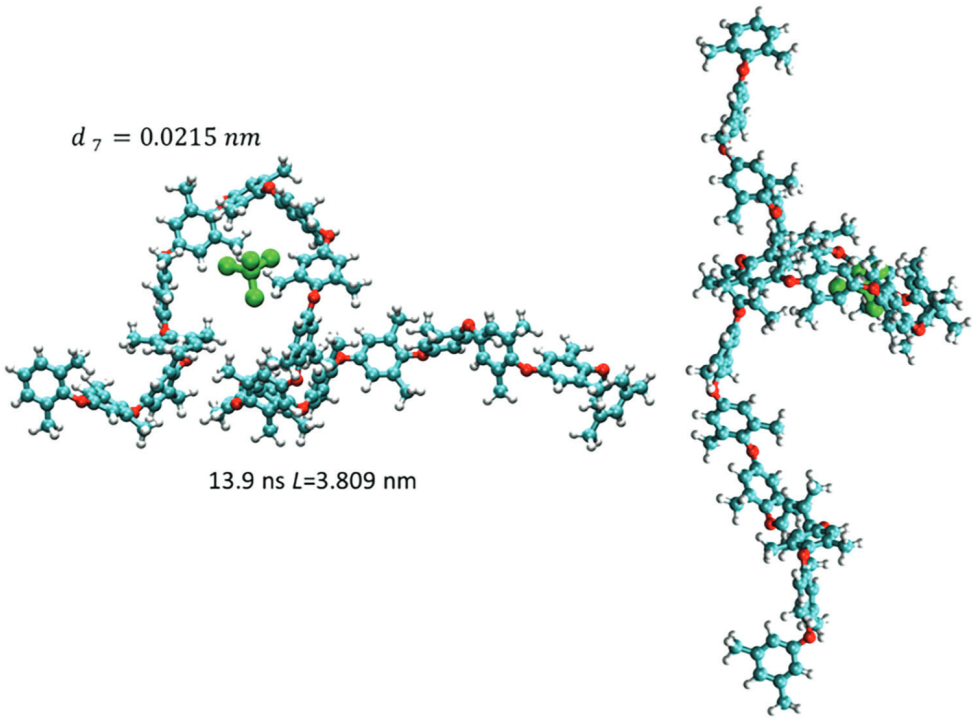

Figure 9. Conformation III of PPO chain together with the CCl_4 molecule hosted in the loop, in two different projections. End-to-end distance L and value for d_7 for the included solvent molecule are also reported. The conformation is observed after 13.9 ns along the MD trajectory.

depicted in **Figure 8**, hosts two solvent molecules, while the second smaller loop is "empty". The loop filled with two molecules involves ten oxygen atoms, while the empty one has six. Also in this case, short distances between chlorine and hydrogen atoms of methyl groups are found for conformation II (ranging from 0.50 to 0.28 nm). Differently from conformation I, chlorine atoms are less tightly packed because there are two solvent molecules in the same loop.

Finally, in **Figure 9** conformation III having one loop containing one solvent molecule is depicted. In addition, also in this case, the loop lies in one plane (this is clear from the side view on the right side of the figure) and involves seven oxygen atoms. In addition, also in this case, short hydrogen-chlorine distances (from 0.44 to 0.27 nm) have been detected.

The average lifetime of loops occupied by one or two solvent molecules (such as the ones detected in conformations I-III) is ≈300 ps, while for the empty loops (such as the one detected in conformation II) is 80 ps.

The establishment of molecular complexes between PPO chain and solvent molecules through the formation of loops gives a molecular explanation of the tendency of PPO to highly coiled conformations as detected from experiments measuring chain dimensions. Moreover, due to the presence of helical conformations hosting solvent molecules in CC structures of PPO, it could be argued that these molecular complexes, already present for a single chain (i.e., at high dilution conditions), can play a relevant role in the nucleation stages preceding the crystallization process of PPO induced by solvents. Polymer chains in solution, or as a polymer melt, are expected to visit many minima of the corresponding potential energy surfaces having small energy differences (of the order of RT). According to this feature, the most stable conformations are the ones minimizing free energy (favoring entropy increase, i.e., the multiplicity of the possible chain and solvent configurations). In this case, a stable situation would correspond to reasonably energetically stable conformations having large multiplicity (i.e., many compatible microscopic states) and the same holds for the solvent configurations. According to this view, folded conformations, hosting one or two molecules in one loop, can be obtained for folded chains in several combinations of dihedral angles and, at same time, allowing more positional entropy of the solvent molecules. Indeed, folded conformations, hosting one or two solvent molecules, are expected to have smaller exposed surface area than the solvent, and then are able to release several solvent molecules. From the polymer point of view, the conformational entropy of an extended chain is lower than a folded one.[64] Moreover, in comparison with looped conformations, more CCl_4 molecules can be solvated around a chain in an open conformation. These features make the open conformations having higher free energy in comparison with coiled ones. This should be the underlying mechanism of the molecular recognition of PPO toward some organic solvents such as CCl_4. A similar entropic mechanism is the thermodynamic basis of protein folding and hydrophobic effect.[65]

According to this view, and in order to give a more quantitative explanation of the behavior observed in MD simulations, structure minimizations starting from several initial configurations of PPO chain in implicit solvent, using the Generalized Born Model (GB/SA in the following)[66–68] considering the guest molecule included into the closed loops or not have been performed. The GB/SA is able to give a quantitative estimation of solvation free energy of the several chain conformations considered for the PPO chain solution and could be a good tool to have

Table 3. Geometry optimizations starting from PPO I, II, III, and IV chain conformations reported in Figure 5. Solvent molecules not included in the loops.

Conformation	I	II	III	IV
G_{polar} [kJ mol^{-1}]	−65.8	−70.9	−69.3	−75.6
$G_{nonpolar}$[kJ mol^{-1}]	113.6	123.4	120.2	129.5
G_{solv}[kJ mol^{-1}]	47.8	52.4	50.8	53.9
SASA [nm^2]	30.0	33.0	32.3	34.1

Table 4. Geometry optimizations starting from PPO I, II, III, and IV chain conformations are reported in Figure 5. Solvent molecules included in the loops.

Conformation	I	II	III
G_{polar} [kJ mol^{-1}]	−64.0	−68.2	−67.7
$G_{nonpolar}$[kJ mol^{-1}]	112.7	119.8	116.7
G_{solv}[kJ mol^{-1}]	48.6	51.6	49.0
SASA [nm^2]	30.6	33.1	32.4

a first confirmation of the hypothesized mechanism. In particular, the total solvation free energy (G_{solv}) can be calculated as the sum of a solvent-solvent cavity term (G_{cav}), a solute-solvent van der Waals term (G_{vdW}), and a solute-solvent electrostatic polarization term (G_{pol}):

$$G_{solv} = G_{cav} + G_{vdW} + G_{pol} \quad (1)$$

GB/SA model computes $G_{cav} + G_{vdW} = G_{nonpolar}$ together by evaluating solvent-accessible surface area (SASA).

Results of geometry optimization, obtained starting from the chain conformations, reported in Figure 5, are reported in **Tables 3** and **4** for the PPO chain and for the PPO chain forming the complex with CCl_4, respectively. As expected, the most coiled conformation I shows the smallest SASA (30 nm^2) and the lowest solvation free energy (47.8 kJ mol^{-1}) among all considered conformations. On the contrary, the most open conformation IV shows the largest SASA (34 nm^2) and the highest solvation free energy (53.9 kJ mol^{-1}). Differences between solvation free energies of the minimized structures favor the looped conformations of an amount ranging from 6.0 to 1.5 kJ mol^{-1} (of the order of *RT*). Moreover, the main contribution to the stabilization of looped conformation comes from $G_{nonpolar}$. In particular, conformation I shows a nonpolar free energy penalty of ≈16 kJ mol^{-1} lower than conformation IV. On the contrary, the polar term stabilizes the open conformation IV of ≈10 kJ mol^{-1} with respect to conformation I. This confirms the entropic nature of the stabilization of looped conformations from both solvation and chain conformational free energy contributions. Similar behavior and comparisons can be made for conformations II and III with respect to conformation IV.

4. Conclusion

The all-atom OPLS force field has been successfully tested for PPO in vacuum against quantum chemical DFT results and in condensed phase using MD simulations of bulk DPE and diluted solution of PPO in CCl_4. A good agreement has been obtained in comparison with available experimental data on chain dimensions and the related conformational statistics. Interestingly the preliminary results obtained for MD simulations in CCl_4 show the formation of stable polymer solvent complexes where the solvent molecule is hosted in closed loops formed by the PPO chains. Estimations of free energy of solvation, made using GB/SA approach, indicate an entropic stabilization of the polymer solvent complexes. The very high similarity of these structures with the intra-helical channels present in the structure of PPO co-crystals suggests a possible connection between the detected host-guest complexes and the nucleation process inducing the crystallization from organic solvents. The role of these solvents, from a microscopic point of view, would be to act during nucleation and successive crystallization through a molecular recognition and/or specific molecular interactions with polymer chains. In this view, the use of OPLS-AA force field, particularly suited for organic liquids, opens the way to a systematic investigation of interactions of PPO and different solvents in solution and possibly to a molecular detailed characterization of the nucleation process.

Supporting Information

Supporting Information is available from the Wiley Online Library or from the author.

Conflict of Interest

The authors declare no conflict of interest.

Data Availability Statement

The data that support the findings of this study are available in the supplementary material of this article.

Keywords

molecular dynamics (MD), polymer crystallization from organic solvents, polymer solvent complexes, PPO

Received: April 21, 2023
Revised: July 26, 2023
Published online: September 5, 2023

[1] J. J. Point, J. P. Demaret, *J. Phys. Chem.* **1987**, *91*, 797.
[2] J. J. Point, C. Coutelier, D. Villers, *J. Phys. Chem.* **1986**, *90*, 3277.
[3] J. J. Point, C. Coutelier, *J Polym Sci Polym Phys* **1985**, *23*, 231.
[4] J. M. Guenet, *Macromolecules* **1986**, *19*, 1961.
[5] J. M. Guenet, G. B. Mckenna, *Macromolecules* **1988**, *21*, 1752.
[6] V. Vittoria, A. R. Filho, F. De Candia, *Polym. Bull.* **1991**, *26*, 445.
[7] P. Sobota, *Macromol. Rapid Commun.* **2005**, *26*, 1589.
[8] J. M. Guenet, *Polymer-Solvent Molecular Compounds*, Elsevier, New York **2010**.
[9] G. Guerra, C. Daniel, P. Rizzo, O. Tarallo, *J. Polym. Sci., Part B: Polym. Phys.* **2012**, *50*, 305.

[10] C. Daniel, S. Longo, R. Ricciardi, E. Reverchon, G. Guerra, *Macromol. Rapid Commun.* **2013**, *34*, 1194.
[11] C. Daniel, J. G. Vitillo, G. Fasano, G. Guerra, *ACS Appl. Mater. Interfaces* **2011**, *3*, 969.
[12] A. Y.u Alentiev, I. S. Levin, M. I. Buzin, N. A. Belov, R. Y.u Nikiforov, S. V. Chirkov, I. V. Blagodatskikh, A. S. Kechekyan, P. A. Kechekyan, V. G. Bekeshev, V. E. Ryzhikh, Y. P. Yampolskii, *Polymer* **2021**, *226*, 123804.
[13] Y. Chatani, Y. Shimane, T. Inagaki, T. Ijitsu, T. Yukinari, H. Shikuma, *Polymer* **1993**, *34*, 1620.
[14] O. Tarallo, V. Petraccone, *Macromol. Chem. Phys.* **2004**, *205*, 1351.
[15] O. Tarallo, V. Petraccone, *Macromol. Chem. Phys.* **2005**, *206*, 672.
[16] P. Pilla, A. Cusano, A. Cutolo, M. Giordano, G. Mensitieri, P. Rizzo, L. Sanguigno, V. Venditto, G. Guerra, *Sensors* **2009**, *9*, 9816.
[17] P. Lova, C. Bastianini, P. Giusto, M. Patrini, P. Rizzo, G. Guerra, M. Iodice, C. Soci, D. Comoretto, *ACS Appl. Mater. Interfaces* **2016**, *8*, 31941.
[18] G. Guerra, G. Milano, V. Venditto, P. Musto, C. De Rosa, L. Cavallo, *Chem. Mater.* **2000**, *12*, 363.
[19] A. R. Albunia, C. D'aniello, G. Guerra, D. Gatteschi, M. Mannini, L. Sorace, *Chem. Mater.* **2009**, *21*, 4750.
[20] A. R. Albunia, G. Milano, V. Venditto, G. Guerra, *J. Am. Chem. Soc.* **2005**, *127*, 13114.
[21] G. Milano, G. Guerra, F. Müller-Plathe, *Chem. Mater.* **2002**, *14*, 2977.
[22] S. Figueroa-Gerstenmaier, C. Daniel, G. Milano, G. Guerra, O. Zavorotynska, J. G. Vitillo, A. Zecchina, G. Spoto, *Phys. Chem. Chem. Phys.* **2010**, *12*, 5369.
[23] C. Liu, K. Kremer, T. Bereau, *Adv Theory Simul* **2018**, *1*, 1800024.
[24] C. Daniel, S. Longo, G. Fasano, J. G. Vitillo, G. Guerra, *Chem. Mater.* **2011**, *23*, 3195.
[25] J. M. Barrales-Rienda, J. M. G. Fatou, *Kolloid-Z. Z. Für Polym.* **1971**, *244*, 317.
[26] S. Horikiri, *J. Polym. Sci. Part -2 Polym. Phys.* **1972**, *10*, 1167.
[27] J. Hurek, E. Turska, *Acta Polym.* **1984**, *35*, 201.
[28] O. Tarallo, V. Petraccone, C. Daniel, G. Fasano, P. Rizzo, G. Guerra, *J. Mater. Chem.* **2012**, *22*, 11672.
[29] P. Rizzo, G. Ianniello, S. Longo, G. Guerra, *Macromolecules* **2013**, *46*, 3995.
[30] C. De Rosa, P. Rizzo, O. De Ballesteros, V. Petraccone, G. Guerra, *Polymer* **1999**, *40*, 2103.
[31] O. Tarallo, M. M. Schiavone, V. Petraccone, C. Daniel, P. Rizzo, G. Guerra, *Macromolecules* **2010**, *43*, 1455.
[32] F. Auriemma, C. Daniel, M. Golla, B. Nagendra, P. Rizzo, O. Tarallo, G. Guerra, *Polymer* **2022**, *258*, 125290.
[33] W. L. Jorgensen, J. Tirado-Rives, *Proc Natl Acad Sci USA.* **2005**, *102*, 6665.
[34] J. R. Fried, M. Sadat-Akhavi, J. E. Mark, *J. Membr. Sci.* **1998**, *149*, 115.
[35] S. K. Singh, L. Kunche, U. Natarajan, *J. Macromol. Sci. Part B.* **2020**, *59*, 796.
[36] A. J. M. Sweere, B. Patham, V. Sugur, J. W. Handgraaf, *Macromol. Theory Simul.* **2020**, *29*, 2000027.
[37] J. Lu, L. C. Jacobson, Y. A. Perez Sirkin, V. Molinero, *J. Chem. Theory Comput.* **2017**, *13*, 245.
[38] M. T. Lee, *J. Phys. Chem. C* **2020**, *124*, 4470.
[39] C. Caleman, P. J. Van Maaren, M. Hong, J. S. Hub, L. T. Costa, D. Van Der Spoel, *J. Chem. Theory Comput.* **2012**, *8*, 61.
[40] M. J Frisch, Gaussian 03. **2004**.
[41] R. Ditchfield, W. J. Hehre, J. A. Pople, *J. Chem. Phys.* **1971**, *54*, 724.
[42] W. J. Hehre, R. Ditchfield, J. A. Pople, *J. Chem. Phys.* **1972**, *56*, 2257.
[43] P. C. Hariharan, J. A. Pople, *Mol. Phys.* **1974**, *27*, 209.
[44] V. A. Rassolov, J. A. Pople, M. A. Ratner, T. L. Windus, *J. Chem. Phys.* **1998**, *109*, 1223.
[45] V. A. Rassolov, M. A. Ratner, J. A. Pople, P. C. Redfern, L. A. Curtiss, *J. Comput. Chem.* **2001**, *22*, 976.
[46] G. A. Petersson, M. A. Al-Laham, *J. Chem. Phys.* **1991**, *94*, 6081.
[47] G. A. Petersson, A. Bennett, T. G. Tensfeldt, M. A. Al-Laham, W. A. Shirley, J. Mantzaris, *J. Chem. Phys.* **1988**, *89*, 2193.
[48] A. D. Becke, *J. Chem. Phys.* **1993**, *98*, 5648.
[49] D. Van Der Spoel, E. Lindahl, B. Hess, G. Groenhof, A. E. Mark, H. J. C. Berendsen, *J. Comput. Chem.* **2005**, *26*, 1701.
[50] W. L. Jorgensen, D. S. Maxwell, J. Tirado-Rives, *J. Am. Chem. Soc.* **1996**, *118*, 11225.
[51] U. Essmann, L. Perera, M. L. Berkowitz, T. Darden, H. Lee, L. G. Pedersen, *J. Chem. Phys.* **1995**, *103*, 8577.
[52] T. Darden, D. York, L. Pedersen, *J. Chem. Phys.* **1993**, *98*, 10089.
[53] D. Van Der Spoel, P. J. Van Maaren, *J. Chem. Theory Comput.* **2006**, *2*, 1.
[54] O. F. Lange, D. Van Der Spoel, B. L. De Groot, *Biophys. J.* **2010**, *99*, 647.
[55] S. Nosé, *Mol. Phys.* **1984**, *52*, 255.
[56] W. G. Hoover, *Phys. Rev. A* **1985**, *31*, 1695.
[57] M. Parrinello, A. Rahman, *J. Appl. Phys.* **1981**, *52*, 7182.
[58] B. Hess, H. Bekker, H. J. C. Berendsen, J. G. E. M. Fraaije, *J. Comput. Chem.* **1997**, *18*, 1463.
[59] B. Hess, C. Kutzner, D. Van Der Spoel, E. Lindahl, *J. Chem. Theory Comput.* **2008**, *4*, 435.
[60] M. Golla, A. Cozzolino, B. Nagendra, E. Vignola, C. Daniel, P. Rizzo, G. Guerra, F. Auriemma, M. C. D'alterio, *Front Chem* **2022**, *9*, 809850.
[61] W. H. Stockmayer, *Makromol. Chem.* **1960**, *35*, 54.
[62] M. Fixman, *J. Chem. Phys.* **1955**, *23*, 1656.
[63] M. Kurata, W. H. Stockmayer, A. Roig, *J. Chem. Phys.* **1960**, *33*, 151.
[64] M. Rubinstein, R. H. Colby, *Polymer Physics*, Oxford University Press, Oxford, **2003**.
[65] R. Phillips, J. Kondev, J. Theriot, H. G. Garcia, N. Orme, *Phys Biol*, 2nd ed.; Garland Science, Boca Raton **2012**.
[66] G. D. Hawkins, C. J. Cramer, D. G. Truhlar, *J. Phys. Chem.* **1996**, *100*, 19824.
[67] D.i Qiu, P. S. Shenkin, F. P. Hollinger, W. C. Still, *J. Phys. Chem. A* **1997**, *101*, 3005.
[68] D. E. Tanner, K. Y. Chan, J. C. Phillips, K. Schulten, *J. Chem. Theory Comput.* **2011**, *7*, 3635.